

Luminescence and site occupancy of Ce^{3+} in $Ba_2Ca(BO_3)_2$

Huihong Lin, Hongbin Liang,^{*,†} Bing Han, Jiuping Zhong, and Qiang Su*

MOE Laboratory of Bioinorganic and Synthetic Chemistry, State Key Laboratory of Optoelectronic Materials and Technologies, School of Chemistry and Chemical Engineering, Sun Yat-Sen University, Guangzhou 510275, People's Republic of China

Pieter Dorenbos and M. Danang Birowosuto

Faculty of Applied Sciences, Delft University of Technology, Mekelweg 15, 2629 JB Delft, The Netherlands

Guobin Zhang, Yibing Fu, and Wenqing Wu

National Synchrotron Radiation Laboratory, University of Science and Technology of China, Hefei 230026, People's Republic of China

(Received 8 May 2007; published 23 July 2007)

The phosphors of Ce^{3+} activated $Ba_2Ca(BO_3)_2$ with chemical formulas $Ba_{2(1-x)}Ce_xNa_xCa(BO_3)_2$ and $Ba_2Ca_{1-2x}Ce_xNa_x(BO_3)_2$ were prepared. The luminescence properties have been investigated under vacuum ultraviolet UV and x-ray excitation. Though the point defects $Ce_{Ba'}$ and $Na_{Ba'}$ are expected to occur in samples $Ba_{2(1-x)}Ce_xNa_xCa(BO_3)_2$, and $Ce_{Ca'}$ and $Na_{Ca'}$ are expected to appear in samples $Ba_2Ca_{1-2x}Ce_xNa_x(BO_3)_2$ according to the formulas of the compounds, however, two types of Ce^{3+} centers were found in all samples due to the occupancy of both Ba^{2+} and Ca^{2+} sites. So the influence of doping concentration on the preferential site occupancy was studied, and it was found that Ce^{3+} ions always preferentially enter Ba^{2+} sites at low doping concentration for both samples $Ba_{2(1-x)}Ce_xNa_xCa(BO_3)_2$ and $Ba_2Ca_{1-2x}Ce_xNa_x(BO_3)_2$. In addition, the $5d$ energy levels and decay behaviors for Ce^{3+} in Ba^{2+} and Ca^{2+} sites, the concentration quenching, and the x-ray excited photon output were evaluated to clearly reveal the luminescence features.

DOI: 10.1103/PhysRevB.76.035117

PACS number(s): 78.60.-b, 61.10.Nz, 78.70.En

I. INTRODUCTION

Because the $f-d$ transitions of Ce^{3+} are parity allowed, they have large absorption cross section and appear as intense bands in spectra, and hence luminescent materials doped with Ce^{3+} absorb the excitation energy efficiently. This parity-allowed feature makes that Ce^{3+} gives intensive emission with a short decay time (~ 20 – 60 ns) in most host lattices. The fast $4f-5d$ transitions of Ce^{3+} in various compounds have drawn attention due to their application in phosphors and scintillators. For example, $(Y, Gd)_3(Al, Ga)_5O_{12}:Ce^{3+}$ absorbs blue light and converts it with high efficiency into yellow emission. The phosphor is now widely used as the yellow component in InGaN-based white-emitting light emitting diodes. $Lu_2SiO_5:Ce^{3+}$ shows a high scintillation light yield of about 26 000 photons per MeV absorbed γ -ray excitation energy, a high density of ~ 7.4 g cm^{-3} , and a short decay time of ~ 40 ns. It is employed in medical imaging detectors for positron emission tomography systems.¹

Ce^{3+} has the $4f^1$ ground state configuration with the first excited states belonging to the $5d$ configuration. The excitation spectrum of Ce^{3+} $5d-4f$ emission provides information on the crystal-field splitting and the centroid energy of the $5d$ states in a host lattice. A similar crystal-field splitting is expected for all lanthanide ions in the same host lattice. That is, when the $5d$ level energies of Ce^{3+} are known in a specific host lattice, they can be used to predict the $5d$ states for the other lanthanide ions in that same lattice. The investigation of the spectroscopic properties of Ce^{3+} in different host lattices is then important not only for possible application but also for basic research.²⁻⁴

Many lanthanides show efficient luminescence in borate compounds, and the spectroscopic properties of lan-

thanides in borates, such as $GdMgB_5O_{10}:Ce^{3+}$, Tb^{3+} , $CaMgB_2O_5:Tb^{3+}$, or $(Y, Gd)BO_3:Eu^{3+}$, were extensively studied.⁵ As for the host lattice alkaline earth orthoborate $Ba_2Ca(BO_3)_2$, the structure of the compound is reported to be similar to that of buetschliite. Verstegen first reported the luminescence of Tb^{3+} in $X_2Z(BO_3)_2$ ($X=Ba, Sr$; $Z=Ca, Mg$).⁶ Keszler and co-workers reported the Eu^{2+} luminescence in the borates $X_2Z(BO_3)_2$ under UV excitation.⁷⁻⁹ Recently, the thermoluminescence characteristics of Tb^{3+} -doped $Ba_2Ca(BO_3)_2$ and Tm^{3+} -, Tb^{3+} -, and Dy^{3+} -doped $Sr_2Mg(BO_3)_2$ were also reported.^{10,11} As a primary work, we have already reported the vacuum ultraviolet visible (vuv-vis) luminescence of $Ba_2Mg(BO_3)_2$ doped with Ce^{3+} and Eu^{2+} ions.¹² To the best of our knowledge, the luminescence of $Ba_2Ca(BO_3)_2:Ce^{3+}$ under vuv and x-ray excitation was not reported. In this work, the vuv-vis spectroscopic properties and the x-ray excited luminescence of $Ba_2Ca(BO_3)_2$ doped with Ce^{3+} ions are investigated. Especially, the site occupancy and the $5d$ energy levels of Ce^{3+} at those different sites (Ca^{2+} or Ba^{2+}) in $Ba_2Ca(BO_3)_2$ will be addressed.

II. EXPERIMENT

A series of powder samples was synthesized by a solid-state reaction technique at high temperature. The reactants include analytical grade pure $BaCO_3$, $CaCO_3$, H_3BO_3 (excess 3 mol % to compensate the evaporation), and 99.95% pure rare earth oxide CeO_2 . Na_2CO_3 was added as a charge compensator because the substitution of a Ce^{3+} ion for an alkaline earth ion requires the presence of a charge compensator to maintain overall charge neutrality of the crystal. According to the nominal compositions of compounds

$Ba_{2(1-x)}Ce_xNa_xCa(BO_3)_2$ and $Ba_2Ca_{1-2x}Ce_xNa_x(BO_3)_2$ ($x = 0.0025, 0.005, 0.0075, 0.01, 0.03, 0.05, 0.07, 0.09, 0.11, 0.13$), appropriate amount of starting materials was thoroughly mixed and ground, and subsequently the mixture was pre-fired at $600\text{ }^\circ\text{C}$ for 1/2 h. After slowly cooling down to room temperature, the pre-fired samples were thoroughly re-ground and then calcined at $950\text{ }^\circ\text{C}$ for 6 h in CO reducing atmosphere. According to the formulas of the compounds, the Kröger-Vink point defects $Ce_{Ba'}$ and $Na_{Ba'}$ will be built up, that is, both Ce^{3+} and Na^+ ions are expected to occur in Ba^{2+} sites for single phase samples $Ba_{2(1-x)}Ce_xNa_xCa(BO_3)_2$ in normal case, while they will appear in Ca^{2+} sites (the point defects $Ce_{Ca'}$ and $Na_{Ca'}$) for single phase samples $Ba_2Ca_{1-2x}Ce_xNa_x(BO_3)_2$, respectively.

The structure of the final products was examined by powder x-ray diffraction (XRD) using $Cu\ K\alpha$ radiation on a Rigaku D/max 2200 vpc x-ray diffractometer. The UV excitation and emission spectra of the phosphors were recorded on a Jobin-Yvon FL3-21 spectrofluorometer at room temperature and a 450 W xenon lamp was used as excitation source. The luminescence decay curves were measured at an Edinburgh FLS 920 combined fluorescence lifetime and steady state spectrometer. The vuv excitation and corresponding luminescent spectra were measured at the vuv spectroscopy experimental station on beam line U24 of National Synchrotron Radiation Laboratory (NSRL). The x-ray excited emission spectra were recorded using an x-ray tube with Cu anode operating at 35 kV and 25 mA. The details of these measurements were described in Refs. 12 and 13.

III. RESULTS AND DISCUSSION

A. Powder x-ray diffraction

The measurements on the powder x-ray diffraction for all samples were performed to verify the phase purity and to check the crystal structure. The XRD patterns of all samples are the same to each other and hence only part of the results is presented in Fig. 1. Curve b shows the XRD patterns of an undoped sample of $Ba_2Ca(BO_3)_2$. It is consistent with the standard card¹⁷ in Fig. 1(a). The XRD patterns of two Ce^{3+} -doped samples $Ba_{2(1-x)}Ce_xNa_xCa(BO_3)_2$ and $Ba_2Ca_{1-2x}Ce_xNa_x(BO_3)_2$ for $x=0.07$ are also shown in Fig. 1, which are labeled as curves c and d, respectively. These two curves are in good agreement with curves a and b, indicating that the rare earth doped samples in the concentration range we investigated are also of single phase and suggesting that the substitution of alkaline earth ions Ba^{2+} and Ca^{2+} by Ce^{3+} and Na^+ does not significantly influence the crystal structure.

B. Emission spectra of $Ba_2Ca(BO_3)_2:Ce^{3+}$ upon vuv-UV excitation

The emission spectra of a series phosphors $Ba_{2(1-x)}Ce_xNa_xCa(BO_3)_2$ and $Ba_2Ca_{1-2x}Ce_xNa_x(BO_3)_2$ ($x = 0.0025, 0.005, 0.0075, 0.01, 0.03, 0.05, 0.07, 0.09, 0.11, 0.13$) were measured. We first present the emission spectra of two Ce^{3+} -doped phosphors $Ba_{2(1-x)}Ce_xNa_xCa(BO_3)_2$ and $Ba_2Ca_{1-2x}Ce_xNa_x(BO_3)_2$ for $x=0.07$ at 20 K and room tem-

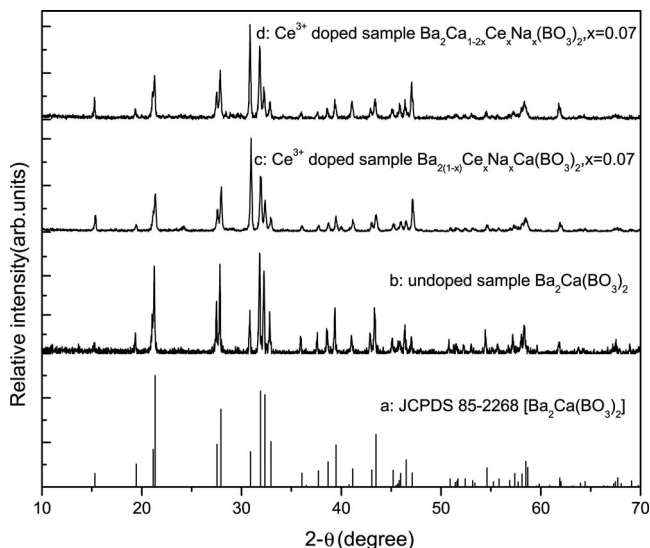


FIG. 1. The XRD patterns of samples $Ba_2Ca(BO_3)_2$ and Ce^{3+} -doped $Ba_2Ca(BO_3)_2$.

perature (RT) under vuv-UV excitation in Figs. 2 and 3.

Usually, Ce^{3+} ions in one specific lattice site will show two emission bands corresponding to the transitions from the lowest $5d$ excited state to the $^2F_{5/2}$ and $^2F_{7/2}$ spin-orbit split $4f$ ground states. The energy separation of the two emission bands coincides with the spin-orbit splitting and amounts to about 2000 cm^{-1} . Often the two bands are resolved much better at lower temperature than at room temperature due to the decrease of the electron-lattice phonon interaction.

The emission spectrum of $Ba_{1.86}Ce_{0.07}Na_{0.07}Ca(BO_3)_2$ upon 182 nm vuv excitation and recorded at 20 K is shown in Fig. 2(a). Here, 182 nm corresponds with the host-related absorption, as will be shown in Sec. III C. Three broad emission bands marked as I ($\sim 382\text{ nm}$), II ($\sim 412\text{ nm}$), and III

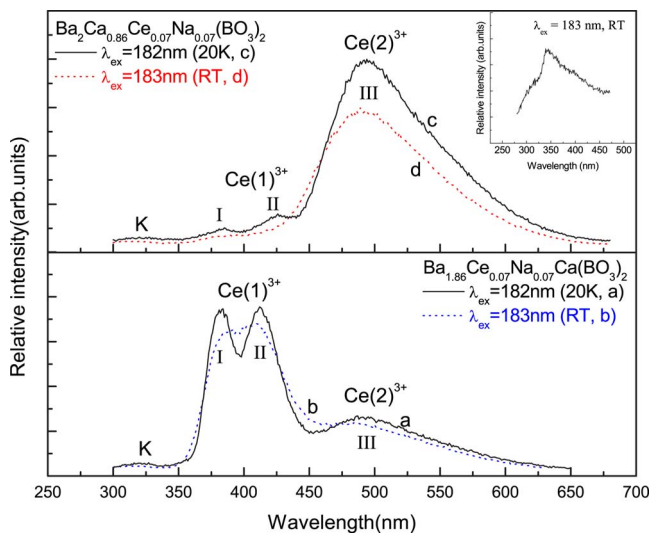


FIG. 2. (Color online) The emission spectrum of $Ba_{1.86}Ce_{0.07}Na_{0.07}Ca(BO_3)_2$ and $Ba_2Ca_{0.86}Ce_{0.07}Na_{0.07}(BO_3)_2$ excited at 182 nm at 20 K and 183 nm at RT. The inset shows the emission spectra of $Ba_2Ca(BO_3)_2$ excited at 183 nm at RT.

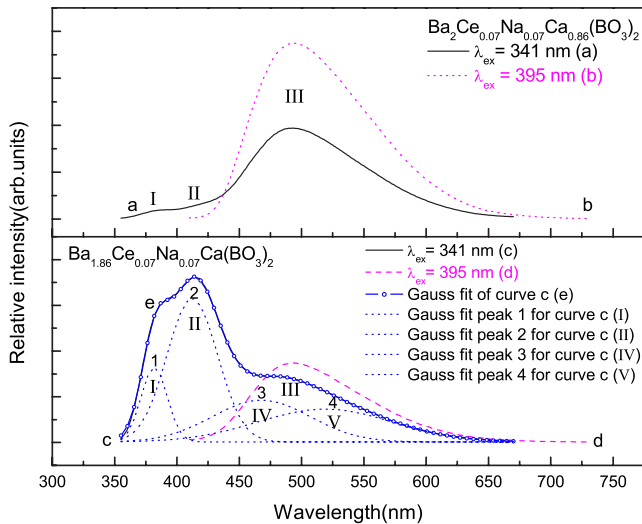


FIG. 3. (Color online) The emission spectra of $\text{Ba}_{1.86}\text{Ce}_{0.07}\text{Na}_{0.07}\text{Ca}(\text{BO}_3)_2$ and $\text{Ba}_2\text{Ca}_{0.86}\text{Ce}_{0.07}\text{Na}_{0.07}(\text{BO}_3)_2$ excited at 341 and 395 nm at RT.

(~ 490 nm) are observed. Bands I and II are attributed to the emission from Ce^{3+} at one specific site. The relatively weak band III is assigned to Ce^{3+} at another site. Before further identifying these two Ce^{3+} sites, we will first consider the crystal structure of the $\text{Ba}_2\text{Ca}(\text{BO}_3)_2$ host compound. The structure of the compound was reported¹⁴ to belong to the monoclinic system with space group $C_{2/m}$. There is only one Ba site which is asymmetrically coordinated by nine oxygen atoms in the C_s symmetry. The Ca atom occupies a slightly distorted octahedral site. When Ce^{3+} ion is incorporated in $\text{Ba}_2\text{Ca}(\text{BO}_3)_2$, it may substitute for Ba^{2+} or Ca^{2+} . We have added Na^+ as charge compensator during synthesis, so the emission of Ce^{3+} in $\text{Ba}_2\text{Ca}(\text{BO}_3)_2:\text{Ce}^{3+}$ will be associated with charge compensated Ce^{3+} centers. When Ce^{3+} enters one specific type of alkaline earth sites (either Ba^{2+} or Ca^{2+} sites), the doped compound will show only one center emission. However, we observe emission from two different luminescent centers in Fig. 2(a). Because the ionic radius of Ce^{3+} is between that of Ba^{2+} and Ca^{2+} , and we conclude that in $\text{Ba}_2\text{Ca}(\text{BO}_3)_2:\text{Ce}^{3+}$, two different luminescent centers are associated with Ce^{3+} on both the Ba^{2+} and Ca^{2+} sites.

In terms of the chemical formula of compound $\text{Ba}_{1.86}\text{Ce}_{0.07}\text{Na}_{0.07}\text{Ca}(\text{BO}_3)_2$ in Fig. 2(a), we consider that most of Ce^{3+} may enter Ba^{2+} sites and believe that stronger bands I and II are associated with the emission of Ce^{3+} in Ba^{2+} sites [i.e., Ce_{Ba} , marked as $\text{Ce}(1)^{3+}$ centers], while weak band III is due to the emission of Ce^{3+} in Ca^{2+} sites [i.e., Ce_{Ca} , marked as $\text{Ce}(2)^{3+}$ centers]. This assignment will be confirmed by another sample $\text{Ba}_2\text{Ca}_{0.86}\text{Ce}_{0.07}\text{Na}_{0.07}(\text{BO}_3)_2$, as shown in the following paragraph. Only a single emission band at about 490 nm was observed from the $\text{Ce}(2)^{3+}$ centers even at 20 K. A possible reason is that the electron-lattice interaction is much stronger for $\text{Ce}(2)^{3+}$ site than that for the $\text{Ce}(1)^{3+}$ site. Spectrum b shows the emission of $\text{Ba}_{1.86}\text{Ce}_{0.07}\text{Na}_{0.07}\text{Ca}(\text{BO}_3)_2$ upon 183 nm excitation at RT. It is similar to spectrum a but bands I and II are not resolved at RT, while they are well resolved

at 382 and 414 nm at 20 K. The thermal quenching results in the decrease of emission intensity at RT for both $\text{Ce}(1)^{3+}$ and $\text{Ce}(2)^{3+}$ centers, as shown in Figs. 2(a) and 2(b).

Spectra c and d in Fig. 2 show the emission of another sample $\text{Ba}_2\text{Ca}_{0.86}\text{Ce}_{0.07}\text{Na}_{0.07}(\text{BO}_3)_2$ upon 182 and 183 nm vuv excitations at 20 K and RT, respectively. In the curves, the weak $\text{Ce}(1)^{3+}$ emission (bands I and II) from Ba^{2+} sites and the strong $\text{Ce}(2)^{3+}$ emission (band III) from Ca^{2+} sites are observed, indicating that most of the Ce^{3+} ions enter Ca^{2+} sites in this sample. Comparing spectra a and b with spectra c and d, it can be found that Ce^{3+} mainly enters Ba^{2+} sites for sample $\text{Ba}_{1.86}\text{Ce}_{0.07}\text{Na}_{0.07}\text{Ca}(\text{BO}_3)_2$, while Ce^{3+} mainly occupies Ca^{2+} sites for sample $\text{Ba}_2\text{Ca}_{0.86}\text{Ce}_{0.07}\text{Na}_{0.07}(\text{BO}_3)_2$.

A band marked as K that peaks at about 320 nm is observed in all spectra of Fig. 2. It is more clearly observed at 20 K than at RT. The band might be attributed to host-related emission, because the emission of the pure host lattice $\text{Ba}_2\text{Ca}(\text{BO}_3)_2$ has a broad band at the same position upon 183 nm excitation at RT, as is shown in the inset of Fig. 2.

In Fig. 3, the emission spectra of samples $\text{Ba}_{1.86}\text{Ce}_{0.07}\text{Na}_{0.07}\text{Ca}(\text{BO}_3)_2$ and $\text{Ba}_2\text{Ca}_{0.86}\text{Ce}_{0.07}\text{Na}_{0.07}(\text{BO}_3)_2$ upon 341 and 395 nm UV excitations are displayed. The excitation wavelengths 341 and 395 nm were chosen, because the absorption band at 341 nm corresponds to the lowest $5d$ state of $\text{Ce}(1)^{3+}$ and the absorption band at 395 nm is due to the lowest $5d$ state of $\text{Ce}(2)^{3+}$, as will be concluded in Sec. III C and Figs. 4 and 5.

For sample $\text{Ba}_2\text{Ca}_{0.86}\text{Ce}_{0.07}\text{Na}_{0.07}(\text{BO}_3)_2$, the emission spectra (curves a and b in Fig. 3) upon 341 and 395 nm excitations are consistent with those in Figs. 2(c) and 2(d). The dominant emission (band III) is from $\text{Ce}(2)^{3+}$ centers. The emission from $\text{Ce}(1)^{3+}$ centers (bands I and II) is very weak.

In Figs. 3(c) and 3(d), the emission spectra of sample $\text{Ba}_{1.86}\text{Ce}_{0.07}\text{Na}_{0.07}\text{Ca}(\text{BO}_3)_2$ are shown. Different spectroscopic features are observed for curves c and d. Upon 395 nm excitation, only a broad emission band III peaking at about 490 nm is observed, and emission from $\text{Ce}(1)^{3+}$ is not present. This suggests that energy transfer from the lowest $5d$ state of $\text{Ce}(2)^{3+}$ to $\text{Ce}(1)^{3+}$ is inefficient. In contrast, when the sample is excited in the lowest $5d$ absorption of $\text{Ce}(1)^{3+}$ at 341 nm, both emissions from $\text{Ce}(1)^{3+}$ (bands I and II) and $\text{Ce}(2)^{3+}$ (band III) occur, see spectrum c, which indicates efficient energy transfer from the lowest $5d$ state of $\text{Ce}(1)^{3+}$ to $\text{Ce}(2)^{3+}$. To determine the emission peak positions for $\text{Ce}(1)^{3+}$ and $\text{Ce}(2)^{3+}$, emission spectrum c was fitted with a sum of four Gaussian profiles (curve e in Fig. 3). The four Gaussian bands are marked as I (~ 382 nm), II (~ 412 nm), IV (~ 468 nm), and V (~ 518 nm). The energy difference is 1906 cm^{-1} between bands I and II and 2062 cm^{-1} between bands IV and V. Both differences are near the expected value of 2000 cm^{-1} between ${}^2F_{5/2}$ and ${}^2F_{7/2}$ of Ce^{3+} .

C. Excitation spectra of $\text{Ba}_2\text{Ca}(\text{BO}_3)_2:\text{Ce}^{3+}$ in the vuv-UV range

The vuv-UV excitation spectra of samples $\text{Ba}_{1.86}\text{Ce}_{0.07}\text{Na}_{0.07}\text{Ca}(\text{BO}_3)_2$ and $\text{Ba}_2\text{Ca}_{0.86}\text{Ce}_{0.07}\text{Na}_{0.07}(\text{BO}_3)_2$

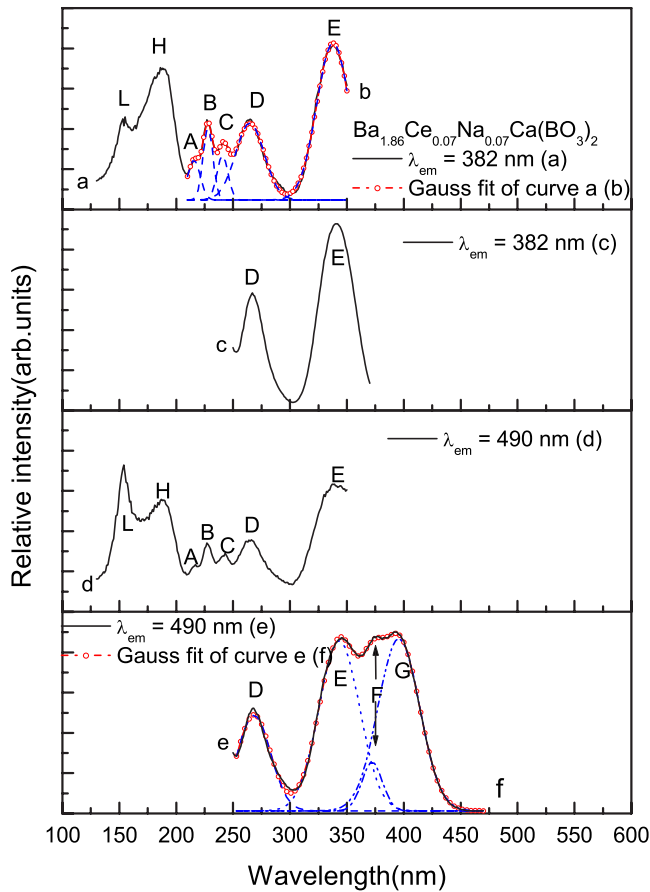


FIG. 4. (Color online) The vuv-UV excitation spectra of $\text{Ba}_{1.86}\text{Ce}_{0.07}\text{Na}_{0.07}\text{Ca}(\text{BO}_3)_2$ at RT. (a) The vuv excitation spectrum of $\text{Ba}_{1.86}\text{Ce}_{0.07}\text{Na}_{0.07}\text{Ca}(\text{BO}_3)_2$ monitoring 382 nm. (b) The Gauss fit of curve a in the range of 210–350 nm. (c) The UV excitation spectrum of $\text{Ba}_{1.86}\text{Ce}_{0.07}\text{Na}_{0.07}\text{Ca}(\text{BO}_3)_2$ monitoring 382 nm. (d) The vuv excitation spectrum of $\text{Ba}_{1.86}\text{Ce}_{0.07}\text{Na}_{0.07}\text{Ca}(\text{BO}_3)_2$ monitoring 490 nm. (e) The UV excitation spectrum of $\text{Ba}_{1.86}\text{Ce}_{0.07}\text{Na}_{0.07}\text{Ca}(\text{BO}_3)_2$ monitoring 490 nm. (f) The Gauss fit of curve e in the 250–470 nm range.

under 382 and 490 nm emissions at RT are displayed in Figs. 4 and 5.

At wavelengths below 200 nm in Figs. 4(a), 4(d), 5(a), and 5(c), two strong absorption bands denoted as H and L are observed. Because the intensity of synchrotron radiation source is relatively weak around 150 nm, it is difficult to confirm the existence or the intensity of band L at about 153 nm. Band H at 183 nm is attributed to the host-related absorption due to the BO_3^{3-} groups. Many BO_3^{3-} -containing borates exhibit absorption around 140–180 nm.^{15,16} The host-related absorption band of $\text{Ba}_2\text{Ca}(\text{BO}_3)_2$ is shifted about 12 nm to longer wavelengths compared to that of $\text{Ba}_2\text{Mg}(\text{BO}_3)_2$ which we reported previously.¹² Apparently, crystal structure and compound formula affect this energy.

Curves a and d in Fig. 4 are the vuv excitation spectra of sample $\text{Ba}_{1.86}\text{Ce}_{0.07}\text{Na}_{0.07}\text{Ca}(\text{BO}_3)_2$ under $\text{Ce}(1)^{3+}$ center emission at 382 nm and $\text{Ce}(2)^{3+}$ center emission at 490 nm, respectively. These two excitation spectra are similar in the range of 130–350 nm. Seven broad bands labeled A, B, C, D, E, H, and L are clearly observed. Because bands A–E are

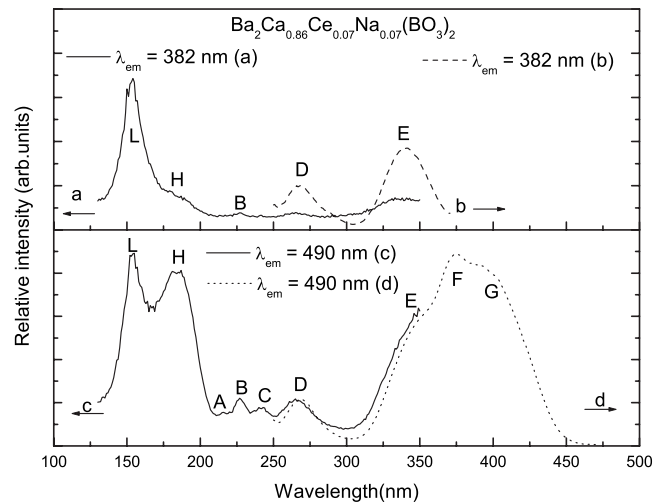


FIG. 5. The vuv-UV excitation spectra of $\text{Ba}_2\text{Ca}_{0.86}\text{Ce}_{0.07}\text{Na}_{0.07}(\text{BO}_3)_2$ at RT. (a) The vuv excitation spectrum of $\text{Ba}_2\text{Ca}_{0.86}\text{Ce}_{0.07}\text{Na}_{0.07}(\text{BO}_3)_2$ monitoring 382 nm. (b) The UV excitation spectrum of $\text{Ba}_2\text{Ca}_{0.86}\text{Ce}_{0.07}\text{Na}_{0.07}(\text{BO}_3)_2$ monitoring 382 nm. (c) The vuv excitation spectrum of $\text{Ba}_2\text{Ca}_{0.86}\text{Ce}_{0.07}\text{Na}_{0.07}(\text{BO}_3)_2$ monitoring 490 nm. (d) The UV excitation spectrum of $\text{Ba}_2\text{Ca}_{0.86}\text{Ce}_{0.07}\text{Na}_{0.07}(\text{BO}_3)_2$ monitoring 490 nm.

relatively weak in the vuv excitation spectra of Figs. 5(a) and 5(c) pertaining to sample $\text{Ba}_2\text{Ca}_{0.86}\text{Ce}_{0.07}\text{Na}_{0.07}(\text{BO}_3)_2$, we consider that these bands are mainly associated with the crystal-field split $5d$ states of the $\text{Ce}(1)^{3+}$ centers (i.e., Ce^{3+} in Ba^{2+} sites). To determine the wavelength of these bands, curve a in the 210–350 nm range was fitted by a sum of five Gaussian functions with maxima at about 216 (band A), 228 (band B), 241 (band C), 265 (band D), and 338 (band E) nm, as shown in Fig. 4.

The UV excitation spectra of 382 and 490 nm emissions for sample $\text{Ba}_{1.86}\text{Ce}_{0.07}\text{Na}_{0.07}\text{Ca}(\text{BO}_3)_2$ at RT are also shown in Fig. 4. They are labeled as curves c and e, respectively. The peak positions are in agreement with those in the vuv excitation spectra (curves a and d) in the 200–350 nm range. A slight redshift of about 2–3 nm is due to differences of the instrument setups used. Different characteristics are observed in the wavelength above 350 nm for Fig. 4(e) under emission at 490 nm. We observed two additional bands labeled as F and G. Figure 4(e) in the 250–470 nm range was fitted with a sum of four Gaussian functions as shown in Fig. 4(f) and marked as D (~268 nm), E (~343 nm), F (~372 nm), and G (~395 nm). We attribute bands F and G to the $4f$ - $5d$ transitions of $\text{Ce}(2)^{3+}$ centers. The $\text{Ce}(1)^{3+}$ centers do not contribute to these bands since they, especially band F, are not present in Fig. 4(c). Therefore, we attribute band G to the excitation of the lowest $5d$ state of $\text{Ce}(2)^{3+}$ centers, and band F is then attributed to the excitation of the second $5d$ state of $\text{Ce}(2)^{3+}$ centers. Excitations of higher energy $5d$ states of $\text{Ce}(2)^{3+}$ overlap and are hidden in the range of bands A–E belonging to $\text{Ce}(1)^{3+}$. We have listed the experimental spectroscopic data in Table I and arrive at the schematic energy levels for $\text{Ce}(1)^{3+}$ and $\text{Ce}(2)^{3+}$ centers, as shown in Fig. 6.

Figure 6 immediately reveals that both $\text{Ce}(1)^{3+}$ and $\text{Ce}(2)^{3+}$ luminescence can be excited via band E by energy

TABLE I. The spectroscopic properties of Ce³⁺ in Ba₂Ca(BO₃)₂.

Property	Value
The first 5 <i>d</i> state of Ce(1) ³⁺ (band E)	~338 nm (~29 586 cm ⁻¹)
The second 5 <i>d</i> state of Ce(1) ³⁺ (band D)	~265 nm (~37 736 cm ⁻¹)
The third 5 <i>d</i> state of Ce(1) ³⁺ (band C)	~241 nm (~41 494 cm ⁻¹)
The fourth 5 <i>d</i> state of Ce(1) ³⁺ (band B)	~228 nm (~43 860 cm ⁻¹)
The fifth 5 <i>d</i> state of Ce(1) ³⁺ (band A)	~216 nm (~46 296 cm ⁻¹)
The emission of Ce(1) ³⁺ center	382 nm, 412 nm
The Stokes shift of Ce(1) ³⁺ emission	3408 cm ⁻¹
The first 5 <i>d</i> state of Ce(2) ³⁺ (band G)	~395 nm (~25 316 cm ⁻¹)
The second 5 <i>d</i> state of Ce(2) ³⁺ (band F)	~372 nm (~26 882 cm ⁻¹)
The emission of Ce(2) ³⁺ center	468 nm, 518 nm
The Stokes shift of Ce(2) ³⁺ emission	3949 cm ⁻¹

transfer from E to F. This is the reason that we observed emission from two Ce³⁺ sites in Figs. 3(a) and 3(c). On the other hand, only Ce(2)³⁺ luminescence will be observed upon excitation in band G. Band G cannot transfer energy to band E, and hence the Ce(1)³⁺ emission is absent in the short-wavelength side of Figs. 3(b) and 3(d). Because the energy can be transferred from the host lattice to both Ce³⁺ centers, we observed the emission from both Ce(1)³⁺ and Ce(2)³⁺ centers upon 182 nm excitation in Fig. 2. The different emission intensities of two types of Ce³⁺ centers in Fig. 2 are mainly the result of different site occupancy ratios for Ce³⁺ in the two different samples, also see Sec. III D.

Figure 5 shows the vuv-UV excitation spectra of 382 and 490 nm emissions of sample Ba₂Ca_{0.86}Ce_{0.07}Na_{0.07}(BO₃)₂ at RT. The results can be interpreted with the scheme in Fig. 6. Because Ce³⁺ mainly enters Ca²⁺ sites [i.e., Ce(2)³⁺ sites] in this sample, excitation bands A–E in Fig. 5(a) are much weaker than those in Fig. 4(a) under emission at 382 nm [Ce(1)³⁺ center emission]. On the other hand, bands D and E are still clearly observed in Fig. 5(b), suggesting that some

Ce³⁺ ions surely occupy Ba²⁺ sites in sample Ba₂Ca_{0.86}Ce_{0.07}Na_{0.07}(BO₃)₂. When monitoring the emission of Ce(2)³⁺ centers at 490 nm, absorption bands A–G are clearly observed in the excitation spectra of Figs. 5(c) and 5(d). Because Ce³⁺ ions mainly enter Ca²⁺ sites in this sample, bands F and G are very strong in curve d. Furthermore, the clear presence of bands A–E in curves c and d confirms that energy transfer from Ce(1)³⁺ to Ce(2)³⁺ centers is efficient.

D. Preferential site occupancy and the concentration quenching of Ce³⁺ in Ba₂Ca(BO₃)₂:Ce³⁺

We measured the emission spectra of a series of samples Ba_{2(1-x)}Ce_xNa_xCa(BO₃)₂ with different doping concentrations ($x=0.0025, 0.005, 0.0075, 0.01, 0.03, 0.05, 0.07, 0.09, 0.11, 0.13$) under excitation in the lowest 5*d* state of Ce(1)³⁺ at 341 nm and the lowest 5*d* state of Ce(2)³⁺ at 395 nm. An example emission spectrum upon 341 nm excitation is shown in Fig. 3(c). For samples Ba_{2(1-x)}Ce_xNa_xCa(BO₃)₂ with different doping concentrations, the following characteristics are observed upon 341 nm excitation in the normalized emission curves a–e of Fig. 7. (1) The emission of two Ce³⁺ centers appears in all samples, especially for the samples with a relatively high Ce³⁺ concentration, which is due to the occupancy of both Ba²⁺ and Ca²⁺ sites by Ce³⁺. (2) The Ce(1)³⁺ center emission is always dominant, suggesting that Ce³⁺ mainly enter the Ba²⁺ lattice sites in samples Ba_{2(1-x)}Ce_xNa_xCa(BO₃)₂. (3) For the samples with different doping concentrations, in order to compare the ratio for Ce³⁺ in two sites, we normalized the integral emission in the range of 355–650 nm for all samples Ba_{2(1-x)}Ce_xNa_xCa(BO₃)₂, as demonstrated in curves a–e in Fig. 7. They directly reveal that the emission intensity ratio of Ce(2)³⁺/Ce(1)³⁺ increases with the increase of Ce³⁺ concentrations, indicating that Ce³⁺ ions preferentially enter Ba²⁺ sites at low doping concentrations, and then the occupancy of Ca²⁺ sites increases with the increase of Ce³⁺ concentrations. (4) It is difficult to determine the quenching concentration of Ce(1)³⁺ accurately because of partial overlap of Ce(1)³⁺ and Ce(2)³⁺ emission bands, as can be seen in spec-

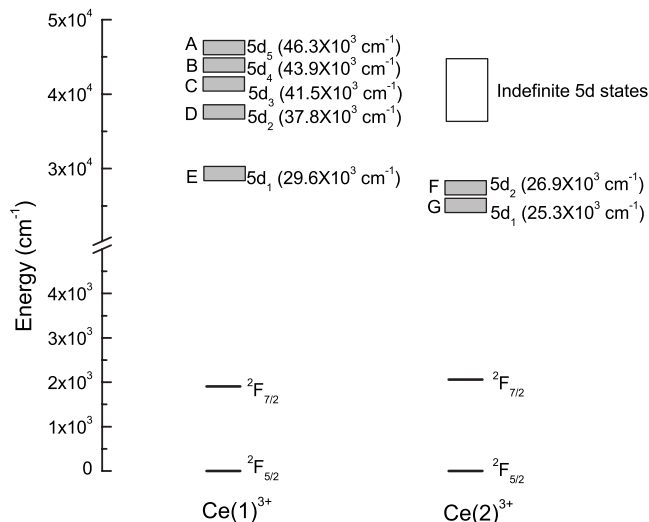


FIG. 6. The energy levels of Ce(1)³⁺ and Ce(2)³⁺ centers in Ba₂Ca(BO₃)₂:Ce³⁺.

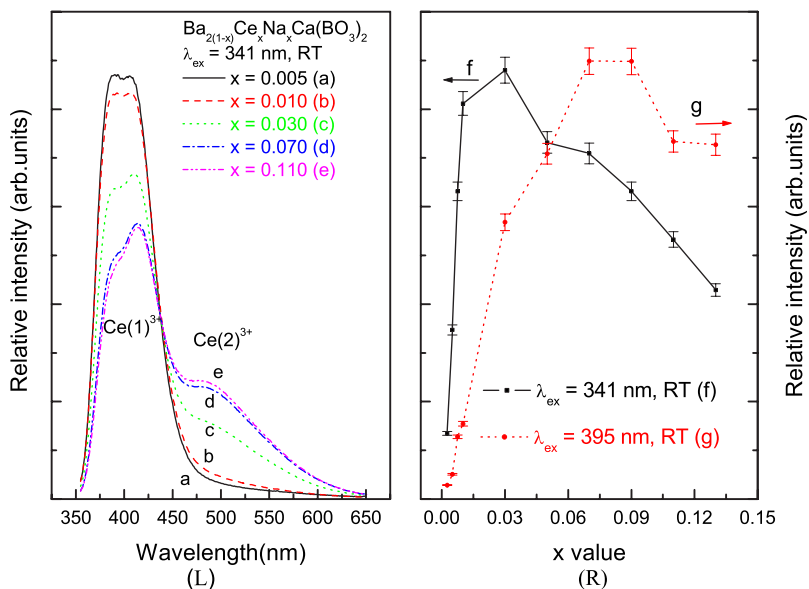


FIG. 7. (Color online) (L) The emission spectra of samples $Ba_{2(1-x)}Ce_xNa_xCa(BO_3)_2$ with different x values at RT. (R) The emission intensity of $Ce(1)^{3+}$ and $Ce(2)^{3+}$ centers on its doping concentration (x) in $Ba_{2(1-x)}Ce_xNa_xCa(BO_3)_2$ samples at RT. [(a)–(e)] The normalized integral emission spectra in the range of 355–650 nm for samples $Ba_{2(1-x)}Ce_xNa_xCa(BO_3)_2$ upon 341 nm excitation. (f) The relative height of $5d \rightarrow {}^2F_{5/2}$ emission at 382 nm on its doping concentration (x) in $Ba_{2(1-x)}Ce_xNa_xCa(BO_3)_2$ samples upon 341 nm excitation. (g) The integral Ce^{3+} emission intensity in the 410–730 nm range on its doping concentration (x) in $Ba_{2(1-x)}Ce_xNa_xCa(BO_3)_2$ samples upon 395 nm excitation.

trum c of Fig. 3. However, Fig. 3(c) shows that the emission of $Ce(2)^{3+}$ is very weak near 382 nm. When we assume that the ratio of the emission intensity between $5d \rightarrow {}^2F_{5/2}$ and $5d \rightarrow {}^2F_{7/2}$ transitions of $Ce(1)^{3+}$ is invariable in different samples, the emission intensity can be used to estimate the $Ce(1)^{3+}$ by the relative height of $5d \rightarrow {}^2F_{5/2}$ emission at 382 nm. Using this method, we estimated the concentration quenching of $Ce(1)^{3+}$ emission upon 341 nm excitation. The results are shown as curve f in Fig. 7. The emission intensity of $Ce(1)^{3+}$ centers first increases with the increase of Ce^{3+} concentrations (x), reaching a maximum around $x=0.03$, and then decreases with increasing concentration due to the concentration quenching and the energy transfer from $Ce(1)^{3+}$ centers to $Ce(2)^{3+}$ centers.

The features for the emission spectra of samples $Ba_{2(1-x)}Ce_xNa_xCa(BO_3)_2$ with different x values upon 395 nm excitation are the same as that in Fig. 3(d). Figure 7 (g) shows the dependence of the integral Ce^{3+} emission intensity in the 410–730 nm range on doping concentrations (x) upon 395 nm excitation. The emission intensity of Ce^{3+} increases with the increase of Ce^{3+} concentrations. For x is between 0.07 and 0.09, Ce^{3+} emission reaches a maximum, and then decreases with increasing Ce^{3+} contents (x).

For comparison, we also systematically investigated the emission spectra of another series of phosphors $Ba_2Ca_{1-2x}Ce_xNa_x(BO_3)_2$ ($x=0.0025, 0.005, 0.0075, 0.01, 0.03, 0.05, 0.07, 0.09, 0.11, 0.13$) upon 341 and 395 nm excitations. The results for one of these samples with $x=0.07$ were already shown in Figs. 3(a) and 3(b), and the other samples show similar spectroscopic characteristics as those in Figs. 3(a) and 3(b).

The preferential site occupancy for Ce^{3+} in $Ba_2Ca_{1-2x}Ce_xNa_x(BO_3)_2$ is revealed with the results in Figs. 8(a)–8(e), where emission of $Ce(1)^{3+}$ and $Ce(2)^{3+}$ sites in samples $Ba_2Ca_{1-2x}Ce_xNa_x(BO_3)_2$ upon 341 nm excitation was displayed. We only present the spectra of five samples. The other samples follow the same trends. Since the integrated emission intensities for each of the emission spectra in

Figs. 8(a)–8(e) are normalized, the relative intensity of $Ce(1)^{3+}$ to $Ce(2)^{3+}$ emission reveals the occupancy of Ce^{3+} over the Ba^{2+} and Ca^{2+} sites. Though Ce^{3+} ions are expected to appear in Ca^{2+} sites according to chemical formulas $Ba_2Ca_{1-2x}Ce_xNa_x(BO_3)_2$, Figs. 8(a) and 8(b) clearly show that at low doping concentration, the dominant emission is from $Ce(1)^{3+}$ instead of $Ce(2)^{3+}$ centers, implying that Ba^{2+} sites are preferentially occupied at low Ce^{3+} concentrations. This behavior is similar to that for samples $Ba_{2(1-x)}Ce_xNa_xCa(BO_3)_2$. The results suggest that Ce^{3+} ions always enter Ba^{2+} sites preferentially at lower doping concentrations, no matter in which types of compounds [$Ba_{2(1-x)}Ce_xNa_xCa(BO_3)_2$ or $Ba_2Ca_{1-2x}Ce_xNa_x(BO_3)_2$]. The larger Ba^{2+} site appears to be favored by Ce^{3+} at low Ce^{3+} concentrations. Then, with the increase of concentration, the emission from Ca^{2+} site is dominant. This dominant emission from $Ce(2)^{3+}$ centers may be explained by two factors. First, the Ca^{2+} site occupancy probably increases with the increase of the doping concentration of Ce^{3+} in the sample. Second, it is also possible that the energy transfer efficiency from $Ce(1)^{3+}$ to $Ce(2)^{3+}$ increases with the increase of doping concentrations. That is to say, with the increase of the energy transfer efficiency, the emission from $Ce(2)^{3+}$ will increase even if the samples of Ca^{2+} sites are not mainly occupied. For these two factors, we consider that the former one may be the chief factor by comparing the emission spectra in Figs. 7(a)–7(e) for samples $Ba_{2(1-x)}Ce_xNa_xCa(BO_3)_2$ with those in Figs. 8(a)–8(e) for samples $Ba_2Ca_{1-2x}Ce_xNa_x(BO_3)_2$ at the same excitation condition. Ce^{3+} ions may mainly occupy Ca^{2+} sites in samples $Ba_2Ca_{1-2x}Ce_xNa_x(BO_3)_2$ at higher doping concentrations. The behavior for these samples is different from that of another type of samples $Ba_{2(1-x)}Ce_xNa_xCa(BO_3)_2$, because Fig. 7 shows that the Ba^{2+} sites are still dominantly occupied with the increase of Ce^{3+} doping concentrations for samples $Ba_{2(1-x)}Ce_xNa_xCa(BO_3)_2$.

In Fig. 8(f), the concentration quenching curve of $Ce(1)^{3+}$ emission upon 341 nm excitation is plotted using the same

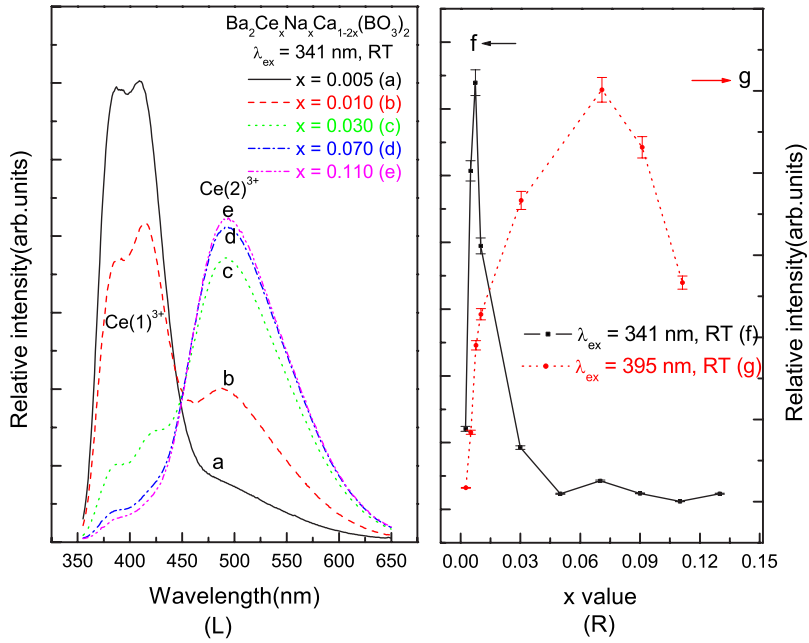


FIG. 8. (Color online) (L) The emission spectra of samples $\text{Ba}_2\text{Ca}_{1-2x}\text{Ce}_x\text{Na}_x(\text{BO}_3)_2$ with different x values at RT. (R) The emission intensity of $\text{Ce}(1)^{3+}$ and $\text{Ce}(2)^{3+}$ centers on its doping concentration (x) in $\text{Ba}_2\text{Ca}_{1-2x}\text{Ce}_x\text{Na}_x(\text{BO}_3)_2$ samples at RT. [(a)–(e)] The normalized integral emission spectra in the range of 355–650 nm for samples $\text{Ba}_2\text{Ca}_{1-2x}\text{Ce}_x\text{Na}_x(\text{BO}_3)_2$ upon 341 nm excitation. (f) The relative height of $5d \rightarrow {}^2F_{5/2}$ emission at 382 nm on its doping concentration (x) in $\text{Ba}_2\text{Ca}_{1-2x}\text{Ce}_x\text{Na}_x(\text{BO}_3)_2$ samples upon 341 nm excitation. (g) The integral Ce^{3+} emission intensity in the 410–730 nm range on its doping concentration (x) in $\text{Ba}_2\text{Ca}_{1-2x}\text{Ce}_x\text{Na}_x(\text{BO}_3)_2$ samples upon 395 nm excitation.

method as for Fig. 7(f). It can be found that the $\text{Ce}(1)^{3+}$ ions with a maximum emission intensity at around $x=0.0075$ in $\text{Ba}_2\text{Ca}_{1-2x}\text{Ce}_x\text{Na}_x(\text{BO}_3)_2$ are smaller than those in $\text{Ba}_{2(1-x)}\text{Ce}_x\text{Na}_x\text{Ca}(\text{BO}_3)_2$.

The concentration quenching of Ce^{3+} emission is also observed upon 395 nm excitation, as shown in Fig. 8(g). We observed similar concentration quenching behavior as for samples $\text{Ba}_{2(1-x)}\text{Ce}_x\text{Na}_x\text{Ca}(\text{BO}_3)_2$ in Fig. 7(g). Under 395 nm excitation, the total emission of Ce^{3+} had a highest intensity when the concentration for Ce^{3+} ions at about $x=0.07$, which is close to that in $\text{Ba}_{2(1-x)}\text{Ce}_x\text{Na}_x\text{Ca}(\text{BO}_3)_2$.

E. Fluorescence decay time of Ce^{3+} in $\text{Ba}_2\text{Ca}(\text{BO}_3)_2:\text{Ce}^{3+}$

Figures 9(a) and 9(b) show the decay curves for $\text{Ba}_{1.86}\text{Ce}_{0.07}\text{Na}_{0.07}\text{Ca}(\text{BO}_3)_2$ and $\text{Ba}_2\text{Ca}_{0.86}\text{Ce}_{0.07}\text{Na}_{0.07}(\text{BO}_3)_2$ luminescence under excitation at 341 and 395 nm and emission at 382 and 490 nm at RT, respectively. The curves were well fitted by a single exponential equation $I_t = A + I_0 \exp(-t/\tau)$, where I_t and I_0 are the luminescence intensity, A is a constant, t is the time, and τ is the decay time. The values of τ are calculated to be 24.0 and 60.6 ns from the fitted curves for $\text{Ce}(1)^{3+}$ and $\text{Ce}(2)^{3+}$ emissions, respectively. The short lifetime is due to Ce^{3+} ions in Ba^{2+} sites and the long value is due to Ce^{3+} ions in Ca^{2+} sites.

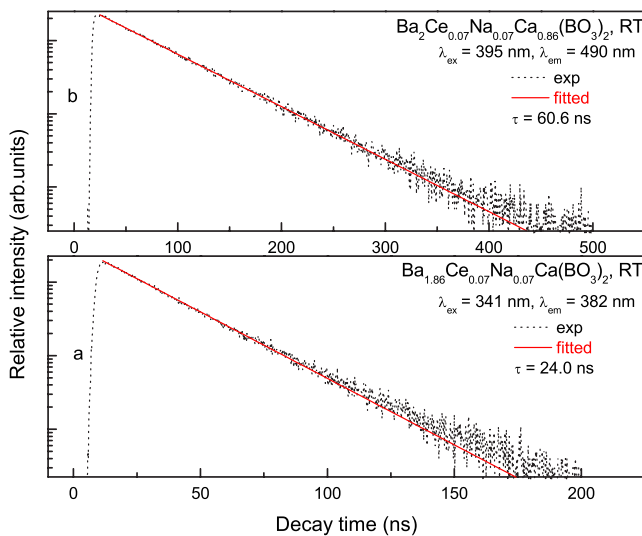


FIG. 9. (Color online) The decay curves of $\text{Ba}_{2(1-x)}\text{Ce}_x\text{Na}_x\text{Ca}(\text{BO}_3)_2$ ($x=0.07$) ($\lambda_{\text{ex}}=341$ nm, $\lambda_{\text{em}}=382$ nm) and $\text{Ba}_2\text{Ca}_{1-2x}\text{Ce}_x\text{Na}_x(\text{BO}_3)_2$ ($x=0.07$) ($\lambda_{\text{ex}}=395$ nm, $\lambda_{\text{em}}=490$ nm) displayed on a logarithmic intensity scale at RT.

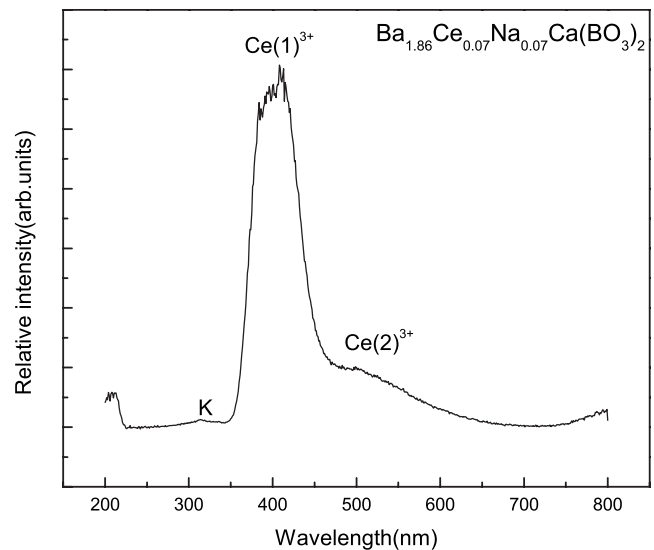


FIG. 10. The x-ray excited emission spectrum of sample $\text{Ba}_{2(1-x)}\text{Ce}_x\text{Na}_x(\text{BO}_3)_2$ ($x=0.07$) at RT.

F. X-ray excited luminescence of $\text{Ba}_2\text{Ca}(\text{BO}_3)_2:\text{Ce}^{3+}$

The x-ray excited emission spectrum of $\text{Ba}_{1.86}\text{Ce}_{0.07}\text{Na}_{0.07}\text{Ca}(\text{BO}_3)_2$ at RT is shown in Fig. 10. We again observe the emission from two Ce^{3+} centers, which are located at the same positions as those observed upon vuv-uv excitation. The band intensity of $\text{Ce}(1)^{3+}$ centers is much stronger than that of $\text{Ce}(2)^{3+}$. This suggests that x-ray excitation favors $\text{Ce}(1)^{3+}$ center emission. The light yield was estimated to be about 5100 ± 370 photons emitted per MeV of absorbed x-ray energy. This value is much smaller than that of $\text{Lu}_2\text{SiO}_5:\text{Ce}^{3+}$ with 26 000 photons MeV^{-1} .

IV. CONCLUSIONS

The spectroscopic properties of a series of phosphors $\text{Ba}_{2(1-x)}\text{Ce}_x\text{Na}_x\text{Ca}(\text{BO}_3)_2$ and $\text{Ba}_2\text{Ca}_{1-2x}\text{Ce}_x\text{Na}_x(\text{BO}_3)_2$ in the vuv-vis range were investigated systematically. From the results, we conclude that the observed excitation and emission bands of Ce^{3+} are due to Ce^{3+} on two different lattice sites, i.e., Ba^{2+} and Ca^{2+} sites in $\text{Ba}_2\text{Ca}(\text{BO}_3)_2$. For Ce^{3+} on Ba^{2+} sites, so-called $\text{Ce}(1)^{3+}$ centers, the excitation bands of the

five crystal-field split $5d$ states are located at 338, 265, 241, 228, and 216 nm. The doublet emission bands of $\text{Ce}(1)^{3+}$ centers are observed at 382 and 412 nm with a Stokes shift of 3408 cm^{-1} . For Ce^{3+} on Ca^{2+} sites, the so-called $\text{Ce}(2)^{3+}$ centers, the first and the second $5d$ states, are observed at 395 and 372 nm. The emission of the $\text{Ce}(2)^{3+}$ centers is at 468 and 518 nm with a Stokes shift of 3949 cm^{-1} . Ce^{3+} ions preferentially occupy Ba^{2+} sites at low doping concentrations, and they start to enter the Ca^{2+} sites when the Ce^{3+} concentration increases. The emission of the short-wavelength $\text{Ce}(1)^{3+}$ centers has a decay time of about 24.0 ns, while that of the long-wavelength $\text{Ce}(2)^{3+}$ centers has 60.6 ns.

ACKNOWLEDGMENTS

This work is supported by the National Natural Science Foundation of China (Grant No. 20571088), by the Science and Technology Project of Guangdong Province (Grants No. 2005A10609001 and No. 2005B10301016), and by the NSRL Innovation Foundation from the Ministry of Education of China (Grant No. 20051251S).

*Authors to whom correspondence should be addressed. FAX: 86-20-84111038

†cesbin@mail.sysu.edu.cn

¹G. Blasse and B. C. Grabmaier, *Luminescent Materials* (Springer-Verlag, Berlin, 1994), Chaps. 6 and 9.

²L. van Pieterse, M. F. Reid, R. T. Wegh, S. Soverna, and A. Meijerink, *Phys. Rev. B* **65**, 045113 (2002).

³P. Dorenbos, *Phys. Rev. B* **64**, 125117 (2001).

⁴P. Dorenbos, *Phys. Rev. B* **62**, 15640 (2000).

⁵S. Shionoga and W. M. Yen, *Phosphor Handbook* (CRC, Boston, 1999).

⁶J. M. P. J. Verstegen, *J. Electrochem. Soc.* **121**, 1631 (1974).

⁷A. Akella and D. A. Keszler, *Mater. Res. Bull.* **30**, 105 (1995).

⁸A. Diaz and D. A. Keszler, *Chem. Mater.* **9**, 2071 (1997).

⁹A. Diaz and D. A. Keszler, *Mater. Res. Bull.* **31**, 147 (1996).

¹⁰L. Y. Liu, Y. L. Zhang, J. Q. Hao, C. Y. Li, Q. Tang, C. X. Zhang,

and Q. Su, *Phys. Status Solidi A* **202**, 2800 (2005).

¹¹L. Y. Liu, Y. L. Zhang, J. Q. Hao, C. Y. Li, Q. Tang, C. X. Zhang, and Q. Su, *Mater. Lett.* **60**, 639 (2006).

¹²H. H. Lin, H. B. Liang, Z. F. Tian, Q. Su, H. Y. Xie, J. F. Ding, G. B. Zhang, and Y. B. Fu, *J. Mater. Res.* **21**, 864 (2006).

¹³Q. Zeng, H. B. Liang, G. B. Zhang, M. D. Birowosuto, Z. F. Tian, H. H. Lin, Y. B. Fu, P. Dorenbos, and Q. Su, *J. Phys.: Condens. Matter* **18**, 9549 (2006).

¹⁴A. Akella and D. A. Keszler, *Main Group Met. Chem.* **18**, 35 (1995).

¹⁵I.-E. Kwon, B.-Y. Yu, H. Bae, Y.-J. Hwang, T.-W. Kwon, C.-H. Kim, C.-H. Pyun, and S.-J. Kim, *J. Lumin.* **87-89**, 1039 (2000).

¹⁶T. Jüstel, J.-C. Krupa, and D. U. Wiechert, *J. Lumin.* **93**, 179 (2001).

¹⁷JCPDS Card No. 85-2268 (unpublished).